

Three-Dimensional Acoustic Turbulence: Weak Versus Strong

E.A. Kochurin^{1,2,*} and E.A. Kuznetsov^{2,3,4}

¹*Institute of Electrophysics, Ural Branch of RAS, 620016, Yekaterinburg, Russia*

²*Skolkovo Institute of Science and Technology, 121205, Moscow, Russia*

³*Lebedev Physical Institute, RAS, 119991, Moscow, Russia*

⁴*Landau Institute for Theoretical Physics, RAS, Chernogolovka, 142432, Moscow region, Russia*

(Dated: July 12, 2024)

Direct numerical simulation of three-dimensional acoustic turbulence has been performed for both weak and strong regimes. Within the weak turbulence, we demonstrate the existence of the Zakharov-Sagdeev spectrum $\propto k^{-3/2}$ not only for weak dispersion but in the non-dispersion (ND) case as well. Such spectra in the k -space are accompanied by jets in the form of narrow cones. These distributions are realized due to small nonlinearity compared with both dispersion/diffraction. Increasing pumping in the ND case due to dominant nonlinear effects leads to the formation of shocks. As a result, the acoustic turbulence turns into an ensemble of random shocks with the Kadomtsev-Petviashvili spectrum.

1. As is known, the developed hydrodynamic turbulence at large Reynolds numbers, $Re \gg 1$, in the inertial interval represents an example of a system with strong nonlinear interaction, when its energy coincides with the interaction Hamiltonian. Another example relates to acoustic turbulence which demonstrates both strong and weak regimes depending on the ratio between nonlinearity and linear wave characteristics. In this sense, acoustic turbulence is much more diverse and richer than hydrodynamic turbulence. When nonlinear interaction of waves is small compared to linear effects, we have a regime of weak turbulence [1] which can be investigated perturbatively by using the random phase approximation. Within the weak turbulence theory (WTT) for arbitrary wave systems, ensembles of waves are described statistically in terms of the corresponding kinetic equations [1, 2]. This theory assumes that each wave with its random phase moves long enough time almost freely and undergoes very rarely small changes due to the nonlinear interaction with other waves. To date, the WTT has been confirmed with high accuracy for dispersive waves (e.g. [3]). The situation changes for acoustic waves without dispersion for which the resonant conditions for three-wave interaction

$$\omega(\mathbf{k}) = \omega(\mathbf{k}_1) + \omega(\mathbf{k}_2), \quad \mathbf{k} = \mathbf{k}_1 + \mathbf{k}_2 \quad (1)$$

are satisfied only for collinear wave vectors \mathbf{k}_i , where $\omega(\mathbf{k}) = kc_s$ is the linear dispersion relation and c_s is the speed of sound. These interacting waves thus form a ray in the k -space. Evidently, translating to the system of coordinates moving with c_s along the ray makes this system strongly nonlinear. In 1D gas dynamics, this nonlinearity leads to the breaking of acoustic waves in accordance with the famous Riemann solution.

However, in a multi-dimensional situation by means of such transition it is possible to exclude c_s only for one given ray, for all other rays propagating under some angles this exclusion does not work. If we take continuously distributed rays with close propagation angles, we

obtain an acoustic beam, which, as is known, is subject to diffraction in the transverse direction. As soon as a ray in the 3D case gets a transverse width, let small, then such a ray will diffract. First time this effect was discussed in the original paper by Zakharov and Sagdeev [4]; practically at the same time the analogous ideas were developed by Newell and Aucoin [5] (see, also [6]). From these arguments follows that the weak turbulence regime for acoustic waves can be realized, as we will show in this Letter, not only in the weak wave dispersion case but also in the dispersionless situation due to the diffraction.

For acoustic waves with weak positive wave dispersion,

$$\omega = kc_s(1 + a^2k^2), \quad (a^2k^2 \ll 1), \quad (2)$$

the resonant conditions (1) are satisfied so that the interacting waves instead of rays form cones with small angles $\sim (ak)^2$ (here a is the dispersion length). The WTT, as known, is applicable for small nonlinearity compared to weak dispersion. In this mode, Zakharov and Sagdeev [4, 7] found exact isotropic solution of the kinetic equation for 3D weak acoustic turbulence

$$E(k) = C_{KZ}(\rho c_s \epsilon)^{1/2} k^{-3/2}, \quad (3)$$

the so-called Zakharov-Sagdeev (ZS) spectrum. Here ϵ is the energy flux towards short wave scales, C_{KZ} is the Kolmogorov-Zakharov (KZ) constant, ρ is density. The power dependence on ϵ in (3) with the exponent 1/2 corresponds to the resonant three-wave interactions (1). In the long-wave limit such a spectrum is local and does not depend on the wave dispersion length a [4, 7]. However, the 2D WT spectrum contains the dependence on a [8].

With increasing pumping the nonlinear interaction becomes comparable to wave dispersion that results in appearance of various coherent phenomena: solitons, collapses, shock waves, etc. (see, e.g. [9]). In this case the system behavior is defined by interaction between coherent structures and their incoherent partners.

In the dispersionless case, when nonlinear effects prevail over diffraction, breaking of the acoustic waves leads

to the formation of shocks. In this regime, according to Kadomtsev and Petviashvili (KP) [10], the acoustic turbulence can be represented as an ensemble of randomly distributed shocks that gives the KP spectrum

$$E(k) = \frac{2S_d c_s^2 \langle \delta \rho^2 \rangle}{\pi \rho} k^{-2}, \quad (4)$$

where S_d is the number of shocks per unit length, $\langle \delta \rho^2 \rangle$ is the mean-square of density jumps at discontinuities (see, e.g. [11]). Notice that exponent of the power-law spectrum (4) is independent on the space dimension. In the 1D case, this is the spectrum of Burgers turbulence [12]. Thus, there are two different approaches to the description of acoustic non-dispersive turbulence predicting different spectra for the same phenomenon.

The main goal of this Letter is to elucidate the reasons for the different behavior of acoustic turbulence spectra by means of direct 3D numerical simulations of the dynamical system. We will show that both spectra (3) and (4) are actually realized, the transition between them being controlled by the level of nonlinearity. Until now there has been no convincing numerical evidence for the realization of both turbulent spectra for 3D acoustic turbulence. Recently, for the weak wave dispersion we have reported some preliminary results of direct simulations of the acoustic WT [13]. In the given Letter, we present the new results mainly concerning statistical properties of this turbulence. Note that, in the dispersionless case, up to now the WT regime has not been numerically observed.

2. Direct numerical simulation of acoustic turbulence has been carried out in the framework of the nonlinear string equation for a scalar function $u(\mathbf{r}, t)$ depending on three spatial coordinates $\mathbf{r} = \{x, y, z\}$ and time t [4, 7]:

$$u_{tt} = \Delta u - 2a^2 \Delta^2 u + \Delta(u^2), \quad (5)$$

where a is the dispersion length, Δ is the Laplace operator. Here, we put $c_s = 1$, and $\rho = 1$. In the linear approximation, the equation (5) has the dispersion law

$$\omega_k^2 = k^2 + 2a^2 k^4, \quad (6)$$

which at $ka \ll 1$ transforms into (2).

The equation (5) can be represented as:

$$u_t = \frac{\delta H}{\delta \phi}, \quad \phi_t = -\frac{\delta H}{\delta u}, \quad (7)$$

where u has the meaning of the density fluctuation and ϕ is of the hydrodynamic potential (the velocity $\mathbf{v} = \nabla \phi$), and the Hamiltonian H is written as

$$\begin{aligned} H &= \frac{1}{2} \int [(\nabla \phi)^2 + u^2] d\mathbf{r} + \int a^2 (\nabla u)^2 d\mathbf{r} + \frac{1}{3} \int u^3 d\mathbf{r} \equiv \\ &\equiv H_1 + H_2 + H_3. \end{aligned} \quad (8)$$

The first term H_1 is the sum of the kinetic and potential energies of linear non-dispersion waves. The second term H_2 is responsible for the wave dispersion, and H_3 describes the nonlinear interaction of waves.

Making the Fourier transform and introducing the normal variables a_k and a_k^* ,

$$u_k = \left(\frac{k^2}{2\omega_k} \right)^{1/2} (a_k + a_{-k}^*), \quad \phi_k = -i \left(\frac{\omega_k}{2k^2} \right)^{1/2} (a_k - a_{-k}^*),$$

equations (7) take the standard form [1, 2]:

$$\frac{\partial a_k}{\partial t} = -i \frac{\delta H}{\delta a_k^*}, \quad (9)$$

where

$$\begin{aligned} H &= \int \omega_k |a_k|^2 d\mathbf{k} + \int V_{k_1 k_2 k_3} (a_{k_1}^* a_{k_2} a_{k_3} + \\ &+ a_{k_1} a_{k_2}^* a_{k_3}^*) \delta(\mathbf{k}_1 - \mathbf{k}_2 - \mathbf{k}_3) d\mathbf{k}_1 d\mathbf{k}_2 d\mathbf{k}_3. \end{aligned}$$

In the nonlinear Hamiltonian H_3 , we left only one resonance term corresponding to decay processes (1). We will take into account the dispersion only in the quadratic part of H and ignore it in the matrix element

$$V_{k_1 k_2 k_3} = \frac{1}{8\pi^{3/2}} (k_1 k_2 k_3)^{1/2}. \quad (10)$$

This expression coincides, up to a constant, with that for acoustic waves [1, 7]. Hence, the kinetic equation for the pair correlator n_k ($\langle a_k^* a_{k_1} \rangle = n_k \delta(\mathbf{k} - \mathbf{k}_1)$) in the WT approximation is written as

$$\frac{\partial n_k}{\partial t} = 2\pi \int d\mathbf{k}_1 d\mathbf{k}_2 (T_{k k_1 k_2} - T_{k_1 k k_2} - T_{k_2 k k_1}), \quad (11)$$

where

$$\begin{aligned} T_{k k_1 k_2} &= |V_{k k_1 k_2}|^2 (n_{k_1} n_{k_2} - n_k n_{k_2} \\ &- n_k n_{k_1}) \delta(\mathbf{k} - \mathbf{k}_1 - \mathbf{k}_2) \delta(\omega_k - \omega_{k_1} - \omega_{k_2}). \end{aligned}$$

The turbulence spectrum $E(k)$ is found from the solution of this equation after angle averaging (see [14, 15])

$$E(k) = \frac{1}{(2\pi)^3} k^2 \omega_k \int n(\mathbf{k}) d\Omega.$$

As was first noted by Zakharov [7], in the kinetic equation (11) in the isotropic case, the dispersion in ω_k can be neglected, despite of a singularity due to the product of two δ -functions which after angle averaging turns out to be integrable. As a result, the kinetic equation admits, except thermodynamic distribution, a stationary power-law solution of the Kolmogorov type: $n_k \propto k^{-9/2}$, which corresponds to the ZS spectrum (3). The KZ constant

within (5) for isotropic turbulence (see Supp. Mat. I [14])

$$C_{KZ} \approx 0.22. \quad (12)$$

The existence of the ZS spectrum in the inertial interval as a spectrum of the Kolmogorov type was numerically confirmed in a number of papers (see, e.g. [16, 17] by solving the kinetic equation (11) only for isotropic distributions. In this Letter, we will show that in direct numerical simulation of 3D acoustic turbulence described by Eq. (11) supplemented by damping at high k and pumping in the region of long waves, the structure of the spectra is not isotropic in the region of small k .

To model turbulence we introduce into the equations (7) both pumping and damping terms:

$$u_t = -\Delta\phi + \mathcal{F}(\mathbf{k}, t) - \gamma_k u, \quad (13)$$

$$\phi_t = -u + 2a^2\Delta u - u^2, \quad (14)$$

where the positive definite operator γ_k responsible for dissipation takes non-zero values at $k \geq k_d$ and the random forcing term $\mathcal{F}(\mathbf{k}, t)$ is narrowly localized in the region of large scales $k \leq k_2$ with a maximum F_0 reached at k_1 ($k_d \gg k_2$). The instantaneous energy dissipation flux $\epsilon_N(t)$ is given as

$$\epsilon_N(t) = L^{-3} \int_{L^3} u \hat{f}^{-1}(\gamma_k u_k) d\mathbf{r}, \quad (15)$$

where \hat{f}^{-1} is the inverse Fourier transform, and L is the system size. In the quasi-stationary state, the energy flux is defined as a mean value $\epsilon = \langle \epsilon_N \rangle = T^{-1} \int_0^T \epsilon_N(t) dt$. The numerical simulation of the Eqs. (13) and (14) is carried out with using accurate pseudo-spectral methods with the total number of Fourier harmonics $N^3 = 512^3$ in a periodic box of size $L^3 = (2\pi)^3$. We set the parameters as follows: $k_1 = 3$, $k_2 = 6$, $k_d = 110$. The details of numerical methods are presented in Supp. Mat. II [14].

3. First, we consider the weakly dispersive regime with $a = 2.5 \cdot 10^{-3}$. Fig. 4 (a) shows the temporal evolution of energy contributions (8). It can be seen the rather quick transition at $t \approx 500$ to the quasi-stationary chaotic regime. Both the dispersive part H_2 and the nonlinear interaction energy H_3 turn out to be small compared to H_1 . The term H_2 exceeds H_3 by almost one order of magnitude, which indicates the realization of a weakly nonlinear regime. The inset to Fig. 4 (a) shows the probability density function (PDF) measured in the quasi-stationary state for the derivative u_x . The PDF is close to a normal Gaussian distribution: the found Skewness $S = \langle u_x^3 \rangle / \langle u_x^2 \rangle^{3/2}$ is near $6.4 \cdot 10^{-3}$, and Kurtosis $K = \langle u_x^4 \rangle / \langle u_x^2 \rangle^2 \approx 3.31$. Deviations of these values from $S = 0$ and $K = 3$ for Gaussian distribution characterize extreme events. The wave action $n(k)$ averaging

over angles shown in Fig. 4 (d) acquires a power-law behavior corresponding to the ZS spectrum with high accuracy (see also the inset for the compensated energy turbulence spectrum). The numerically found KZ constant $C_{KZ} \approx 0.24$ is close to the theoretical prediction (12) (for more details Sec. III of Sup. Mat. [14]). To our knowledge, this is the first direct calculation of the KZ constant for 3D acoustic turbulence.

4. The second numerical experiment is aimed to verify the possible realization of WT regime in the absence of dispersion. Fig. 4 (b) shows that the system reaches the quasi-stationary state approximately at the same time ($t \approx 500$) as in the weakly dispersive case. The energy pumping intensity F_0 was the same for both experiments, $F_0 = 1.25 \cdot 10^{-3}$. The nonlinear interaction term H_3 turns out to be in three orders of magnitude less than H_1 . The PDF shown in the inset to Fig. 4 (b) is close to Gaussian distribution with Skewness $S \approx 4.9 \cdot 10^{-2}$ and Kurtosis $K \approx 3.47$. Fig. 4 (e) shows the turbulence spectrum for non-dispersive regime $a = 0$: n_k spectrum turns out in very well agreement with the power-law distribution, $\propto k^{-9/2}$. The estimation for KZ constant gives $C_{KZ} \approx 0.1$, i.e. still has the same order with KZ constant (12).

Thus, upon the transition to a purely non-dispersive regime, the system demonstrates weakly turbulent behavior with the ZS spectrum (3). A fundamental question arises: what is the mechanism for the generation of weak acoustic turbulence in the absence of wave dispersion? Some differences between two regimes are seen in Fig. 5 (a) and (e): the distribution of $u(\mathbf{r})$ in the weak dispersion (WD) case is smoother compared to that of $a = 0$. For the Fourier spectra $|u_k|$ in $k_z = 0$ plane (Fig. 5 (b) and (f)), the difference becomes more observable. First, for the WD case narrow jets form in the region of small k ([13]). These jets widen with increasing k due to wave dispersion, and respectively the distribution becomes more isotropic. Unlike WD, at $a = 0$ the spectrum $|u_k|$ consists of a discrete set of narrow jets of the conic type which do not intersect each other (see Fig. 5 (c) and (g)). The corresponding isosurfaces of Fourier spectra $|u_k|$ shown in the Fig. 5 (c) and (g) have the hedgehog form for which observed rays (needles) appear as a result of three-wave nonlinear interaction (1).

5. To clarify the WT mechanism in the non-dispersive (ND) regime, we separate a jet directed along the x axis by means of filtering (for details, see Sup. Mat. IV [14]). For such (narrow) jet, the dispersion relation (2) ($a = 0$) can be expanded into a series relatively the small parameter $\Omega_0 = (k_\perp/k_x)$ (angle at the apex of a cone directed along the x axis)

$$\omega_k = |\mathbf{k}| \approx k_x (1 + \Omega_0^2/2),$$

so that H_1 represents a sum of two terms $H_1 = \int \omega_k n(k) d\mathbf{k} \approx \int [k_x + \Omega_0^2 k_x/2] n(k) d\mathbf{k} = H_\parallel + H_\perp$, where H_\parallel corresponds to the energy of acoustic beam propagating along x direction and H_\perp defines its diffraction

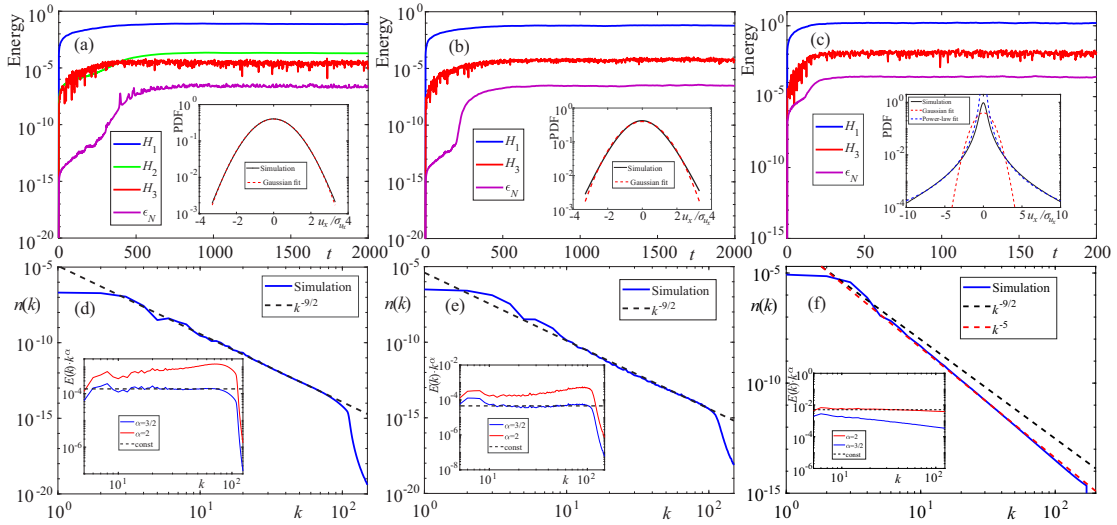


FIG. 1: Energy contributions (8) and dissipation flux (15) as functions of time for $a = 2.5 \cdot 10^{-3}$ (a) and for $a = 0$ (b) and (c). The insets show PDF for u_x rescaled by its standard deviation σ_{u_x} . Red dashed lines correspond to a Gaussian fit and blue dashed line is the power-law fit $|u_x/\sigma_{u_x}|^3$. The spatial spectra of wave action $n(k)$ are shown in the quasi-stationary state for $a = 2.5 \cdot 10^{-3}$ (a) and for $a = 0$ (b) and (c). The insets are the compensated turbulence energy spectra.

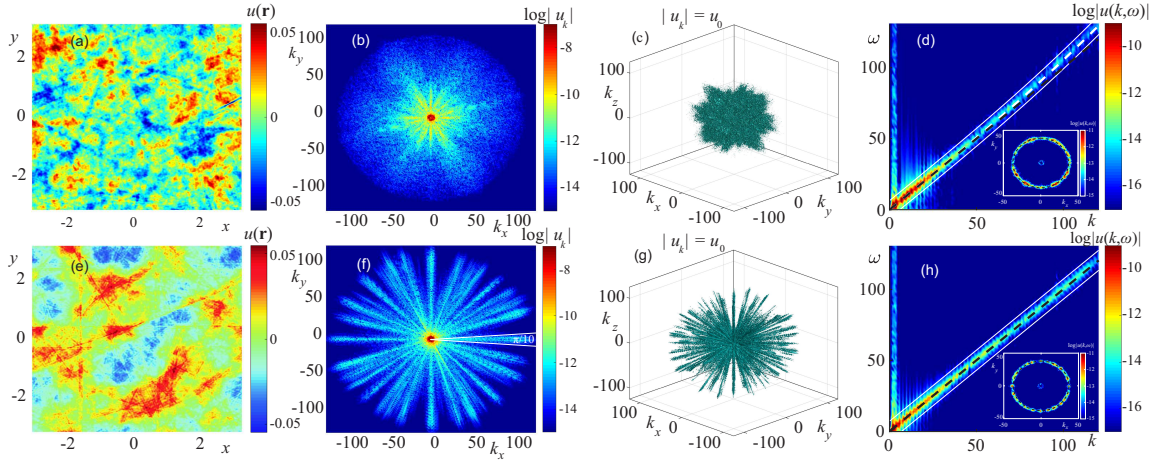


FIG. 2: (a),(e): Dependence $|u(x,y)|$ at $z = 0$ - plane at $t = 2000$; (b), (f): Fourier spectra of $|u(\mathbf{k})|$ as function of k_x and k_y at $k_z = 0$ plane at $t = 2000$; (c),(g): Isosurfaces of the Fourier spectra $|u_{\mathbf{k}}| = 5 \cdot 10^{-6}$ (in the 'hedgehog' form); (d), (h): The space-time Fourier transform $|u(\mathbf{k}, \omega)|$, black and white dashed lines correspond to the non-dispersive (2) and WD (6) wave propagation, respectively, white solid lines show the nonlinear frequency broadening $\delta\omega$. The insets show $|u(\mathbf{k}, \omega_0)|$ with $\omega_0 = 40$ on $k_z = 0$ plane; (a)-(d) and (e)-(h) correspond to $a = 2.5 \cdot 10^{-3}$ and $a = 0$, respectively.

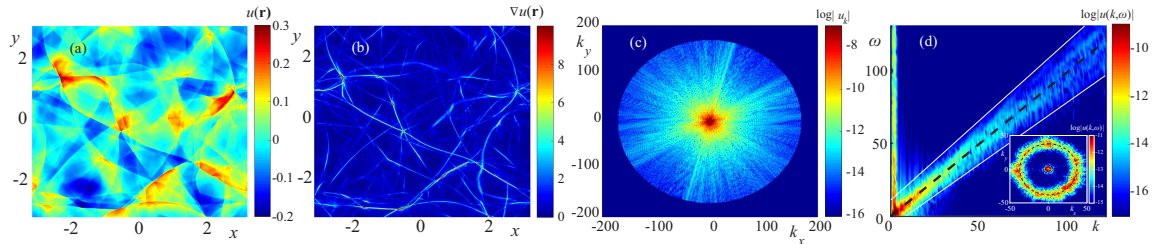


FIG. 3: (a), (b): Dependences $|u(\mathbf{r})|$ and $|\nabla u(\mathbf{r})|$ on the plane $z = 0$ for shock-wave regime, $t = 200$. (c): Fourier spectrum $|u_{\mathbf{k}}|$ in the $k_z = 0$ plane is shown at $t = 200$. (d): The space-time Fourier transform $|u(\mathbf{k}, \omega)|$, the black dashed line corresponds to the non-dispersive wave propagation, (2). White solid lines demonstrate the nonlinear frequency broadening $\delta\omega$. The inset shows $|u(\mathbf{k}, \omega_0)|$ with $\omega_0 = 40$ in $k_z = 0$ section.

energy. To calculate these contributions, we filtered the function $u(\mathbf{k})$ in a narrow cone along k_x . Note that one

selected cone (jet) occupies approximately angle about $\pi/10$, see Fig. 5 (f). Thus, the energy contributions have a ratio $H_{\perp}/H_{\parallel} \approx 0.05$. Direct calculation gives $H_{\perp} \approx 4.3 \cdot 10^{-5}$, whereas the nonlinear interaction energy for the selected jet is estimated as $H_3 \approx 3.7 \cdot 10^{-7}$. Thus, for the given jet the diffraction energy is in two orders of magnitude larger nonlinear interaction energy that explains appearance of the weak acoustic turbulence and the ZS spectrum (3). The space-time Fourier transforms $|u(\mathbf{k}, \omega)|$ shown in the Fig. 5 (d) and (h) also indicate the weakly nonlinear evolution. The figure does not reveal the influence of any coherent and strongly nonlinear structures. Only a slight frequency broadening δ_{ω} is observed.

Thus, weak acoustic turbulence can be realized in both weak dispersion and non-dispersive cases. The criterion of WT in both regimes in some sense is the same: the dispersion and/or diffraction effects should prevail non-linearity, which for acoustic waves is responsible for their breaking.

6. In the third numerical simulation, we investigate strong acoustic turbulence in the non-dispersive case. To demonstrate such regime we consider a situation of extremely large pumping amplitude when F_0 was increased to $40 \cdot 10^{-3}$, i.e., by more than an order of magnitude larger in comparison with two previous numerical experiments. Secondly, to suppress the “bottleneck” effect we set $k_d = 1$, that provides the energy dissipation in all ranges of k (see Sup. Mat. V [14]).

For such conditions we observed a very rapid approaching to the stationary state, $t \approx 50$, see Fig. 4 (c). In the inset, one can see that the PDF is very different from the Gaussian distribution with highly elongated non-Gaussian tails indicating the presence of extreme events. Kurtosis reaches a very large value $K \approx 46.37$. Skewness is estimated as $S \approx 0.28$. Thus, the PDF demonstrates a high level of intermittency in the system. The turbulence spectrum for this strongly nonlinear regime is shown in Fig. 4 (f): the exponent of $n(k)$ is very close to -5 corresponding to KP spectrum (4), the energy spectrum $E(k) \sim k^{-2}$ is shown at the inset.

Fig. 6 (a) and (b) show the spatial distributions of $u(\mathbf{r})$ and its gradient $\nabla u(\mathbf{r})$ at the $z = 0$ plane which demonstrate the presence of a set of shock waves propagating under various angles. The spatial turbulent spectrum shown in Fig. 6 (c) clearly indicates the quasi-isotropic behavior of wave energy in Fourier space. Thus, with increasing the nonlinearity level, we observe a transition to the state with strong intermittency. Fig. 6 (d) shows the space-time Fourier spectrum of $u(\mathbf{r}, t)$ that allows us to estimate the frequency broadening $\delta_{\omega} = 1/\tau_{NL}$, where τ_{NL} is characteristic nonlinear time. We have computed the parameter τ_L/τ_{NL} with characteristic linear diffraction time $\tau_L = [\Omega_0^2 k/2]^{-1}$ for both weak and strong WT regimes, see Sup. Mat. VI [14]. Comparison of these times shows that in the strong turbulence regime, τ_L/τ_{NL}

is about 5. The latter means that the wave breaking is more rapid process leading to formation of shocks randomly distributed due to the chaotic pumping. This is a reason for the appearance of the KP spectrum [10].

7. The main result of the work is that the ZS spectrum of 3D weak acoustic turbulence (3) can indeed be realized in both WD and ND regimes. The mechanism for the development of WT is the divergence (diffraction) of acoustic waves preventing their breaking. However, under action sufficiently large pumping, acoustic turbulence turns into an ensemble of random shocks described by the KP spectrum (4). Thus, the spectra (3) and (4) correspond to different limiting cases of the weakly and strongly nonlinear regimes of 3D acoustic turbulence.

The authors are grateful to V.E. Zakharov for very fruitful discussions at the earlier stage of performance of this work. We also thank P.-L. Sulem for one valuable remark. This work was supported by the Russian Science Foundation (grant no. 19-72-30028).

SUPPLEMENTAL MATERIAL TO “THREE-DIMENSIONAL ACOUSTIC TURBULENCE: WEAK VERSUS STRONG”

In this Supplemental Material, we present additional data analysis related to theoretical and numerical study of the three-dimensional acoustic turbulence: weak turbulence theory for 3D acoustic waves (Sec. I), details of the numerical model (Sec. II), estimations for the Kolmogorov-Zakharov constants for both weakly dispersive and pure non-dispersive regimes (Sec. III), analysis of a separate jet of the function $u(\mathbf{k})$ in Fourier space (Sec. IV), details for the suppression of “bottleneck” effect arising for high level of nonlinearity (Sec. V), and characteristic nonlinear time comparison for weakly and strongly turbulent regimes of motion (Sec. VI).

WEAK TURBULENCE THEORY FOR 3D ACOUSTIC WAVES

Consider the wave kinetic equation (11, main text) with the matrix element (10, main text). As was first noted by Zakharov [7], in the kinetic equation (11, main text) in the isotropic case, the dispersion in ω_k at $k \rightarrow 0$ can be neglected, despite of a singularity due to the product of two δ -functions which after angle averaging turns out to be integrable. As a result, the kinetic equation admits, except thermodynamic distribution, a stationary power-law solution of the Kolmogorov type: $n_k \propto k^{-9/2}$, which corresponds to the ZS spectrum $E(k) \propto k^{-3/2}$. Multiplying (11, main text) by $4\pi k^3 \frac{1}{(2\pi)^3}$ with account that angle average $\langle \delta(\mathbf{k} - \mathbf{k}_1 - \mathbf{k}_2) \rangle = 2\pi/(kk_1k_2)$, we get

$$\frac{\partial E(k)}{\partial t} = \frac{1}{32\pi^3} k \int dk_1 dk_2 (W_{kk_1k_2} - W_{k_1kk_2} - W_{k_2kk_1}) \quad (16)$$

where

$$W_{kk_1k_2} = k^2 k_1^2 k_2^2 (n_{k_1} n_{k_2} - n_k n_{k_2} - n_k n_{k_1}) \delta(k - k_1 - k_2).$$

Because of $\int E(k) dk = \text{const}$ the equation (16) can be rewritten as a conservation law:

$$\frac{\partial E(k)}{\partial t} + \frac{\partial P}{\partial k} = 0$$

where P is the energy flux which is found after integration of the left-hand side of (16) over k

$$\frac{\partial P}{\partial k} = -\frac{k}{32\pi^3} \int dk_1 dk_2 (W_{kk_1k_2} - W_{k_1kk_2} - W_{k_2kk_1}). \quad (17)$$

Let $n_k = Ak^x$ where x is unknown exponent. It gives for the quantity $\frac{\partial P}{\partial k}$ a power-law function

$$\frac{\partial P}{\partial k} = k^y I; \quad y = 2x + 8 \quad (18)$$

where I is a constant depending on y . Hence we have

$$P = \frac{k^{y+1}}{y+1} I. \quad (19)$$

Note, independence P on k takes place at $y = -1$ (where $I = 0$!) that corresponds to the exact stationary solution of Eq. (11, main text) in the form of the Zakharov-Sagdeev spectrum:

$$E(k) \propto k^{-3/2}.$$

In order to find dependence I on x let us make Zakharov transformation in the second and the third terms of (17):

$$\begin{aligned} k_1 &= k \frac{k}{k'}, \quad k = k' \frac{k}{k'}, \quad k_2 = k'' \frac{k}{k'}; \\ k_2 &= k \frac{k}{k''}, \quad k = k'' \frac{k}{k''}, \quad k_1 = k' \frac{k}{k''}. \end{aligned}$$

This gives

$$\frac{\partial P}{\partial k} = -\frac{A^2 k}{32\pi^3} \int dk_1 dk_2 k^2 k_1^2 k_2^2 \left[1 - \left(\frac{k}{k_1} \right)^y - \left(\frac{k}{k_2} \right)^y \right] (kk_1k_2)^x [k^{-x} - k_1^{-x} - k_2^{-x}] \delta(k - k_1 - k_2). \quad (20)$$

Note that stationary KZ spectrum takes place when

$$y = -1, \text{ or } x = -9/2.$$

Then integration of Eq. (20) relative to k_2 yields

$$\frac{\partial P}{\partial k} = -\frac{A^2}{32\pi^3} k \int_0^k dk_1 k^2 k_1^2 (k - k_1)^2 \left[1 - \left(\frac{k}{k_1}\right)^y - \left(\frac{k}{k - k_1}\right)^y \right] [kk_1(k - k_1)]^x [k^{-x} - k_1^{-x} - (k - k_1)^{-x}].$$

In terms of new variable $\xi = k_1/k$ ($0 \leq \xi \leq 1$), this expression takes the form:

$$\frac{\partial P}{\partial k} = -\frac{A^2}{32\pi^3} k^y \int_0^1 d\xi \left[1 - \left(\frac{1}{\xi}\right)^y - \left(\frac{1}{1-\xi}\right)^y \right] [\xi(1-\xi)]^{x+2} [1 - \xi^{-x} - (1-\xi)^{-x}]$$

where

$$I(y) = -\frac{A^2}{32\pi^3} \int_0^1 d\xi \left[1 - \left(\frac{1}{\xi}\right)^y - \left(\frac{1}{1-\xi}\right)^y \right] [\xi(1-\xi)]^{x+2} [1 - \xi^{-x} - (1-\xi)^{-x}]$$

Now putting in (20) $y = -1 + \alpha$ and considering the limit $\alpha \rightarrow 0$ result in the following expression for the energy flux ($P_{st} = \varepsilon$):

$$\begin{aligned} \varepsilon &= \frac{A^2}{32\pi^3} \Lambda, \\ \Lambda &= \int_0^1 d\xi \left[\xi \ln \left(\frac{1}{\xi}\right) + (1-\xi) \ln \left(\frac{1}{1-\xi}\right) \right] [\xi(1-\xi)]^{-5/2} [1 - \xi^{9/2} - (1-\xi)^{9/2}]. \end{aligned} \quad (21)$$

Here the convergent integral $\Lambda > 0$ provides the positive energy flux, directed to the small scale region. Note also, that convergence of the integral means the locality of the spectrum.

Hence

$$A = 4\pi \left(\frac{2\pi\varepsilon}{\Lambda} \right)^{1/2}$$

and respectively the ZS spectrum takes the form

$$E(k) = \left(\frac{8\varepsilon}{\pi\Lambda} \right)^{1/2} k^{-3/2}$$

where the Kolmogorov-Zakharov constant is equal to

$$C_{KZ} = \left(\frac{8}{\pi\Lambda} \right)^{1/2}$$

with $\Lambda = 52.42$. Thus, in the isotropic case we have $C_{KZ} \approx 0.22$.

NUMERICAL MODEL AND PARAMETERS

Numerical integration of the system of equations (12, main text) and (13, main text) was carried out in a cubic domain $(2\pi)^3$ with periodic boundary conditions over all three coordinates. Time integration was performed using an explicit scheme by means of the Runge-Kutta method of fourth order accuracy with step $dt = 5 \cdot 10^{-3}$. The equations were integrated over spatial coordinates using pseudo-spectral methods with the total number of harmonics $N^3 = 512^3$. To calculate the fast Fourier transform, parallel computing technology CUDA on graphics processors (GPU) was used. To suppress the aliasing effect, we used a filter that nulls higher harmonics with a wavenumber above $k_a \geq N/3$. The operator γ_k responsible for dissipation and the forcing term $\mathcal{F}(\mathbf{k}, t)$ arising in (12, main text) and (13, main text) are given in Fourier space as:

$$\begin{aligned} \gamma_k &= 0, \quad k \leq k_d, \\ \gamma_k &= \gamma_0(k - k_d)^2, \quad k > k_d, \\ \mathcal{F}(\mathbf{k}, t) &= F(k) \cdot \exp[iR(\mathbf{k}, t)], \\ F(k) &= F_0 \cdot \exp[-\lambda_0^4(k - k_1)^4], \quad k \leq k_2, \\ F(k) &= 0, \quad k > k_2. \end{aligned}$$

Here $R(\mathbf{k}, t)$ are random numbers uniformly distributed in the interval $[0, 2\pi]$, γ_0 and F_0 are constants.

The work presents three series of calculations for different regimes of acoustic turbulence. The first calculation series is made to show the possibility of realization of a weakly dispersive regime of weak acoustic turbulence with small enough dispersion parameter, $a = 2.5 \cdot 10^{-3}$. The second series presents pure non-dispersive regime with $a = 0$ but keeping the nonlinearity level small. Finally, the third calculation experiment is carried out for non-dispersive wave regime but with sufficiently high level of energy pumping to show the transition to a strongly nonlinear regime of motion.

The dispersion length a for the first experiment was chosen as $a = 2.5 \cdot 10^{-3}$. The maximum dispersion addition at the end of the inertial interval, $k = k_d$, was $(k_d a)^2 \approx 0.1$. Other parameters were: $k_d = 110$, $k_1 = 3$, $k_2 = 6$, $\lambda_0 = 0.64$, $\gamma_0 = 10^{-1}$, $F_0 = 1.25 \cdot 10^{-3}$. With this choice of parameters, the inertial interval was more than one decade. For the second numerical experiment we set, $a = 0$, all other parameters except, $\gamma_0 = 10^{-2}$, were the same as for the case of weak dispersion. The third series of calculations was made for the pure non-dispersive regime but the quantity F_0 increased from $1.25 \cdot 10^{-3}$ to $40 \cdot 10^{-3}$, i.e., by more than an order of magnitude. The selected value of F_0 is the maximal for our numerical setup, since the width of the forming shocks becomes comparable with the grid step. With such a large pumping amplitude, a “bottleneck” effect is observed, which leads to wave energy accumulation near the dissipation region k_d . To suppress the effect, we set $k_d = 1$, i.e., the energy dissipation occurs in all ranges of wavenumbers. Other parameters that changed in this case were: $dt = 2.5 \cdot 10^{-3}$, $\gamma_0 = 10^{-4}$.

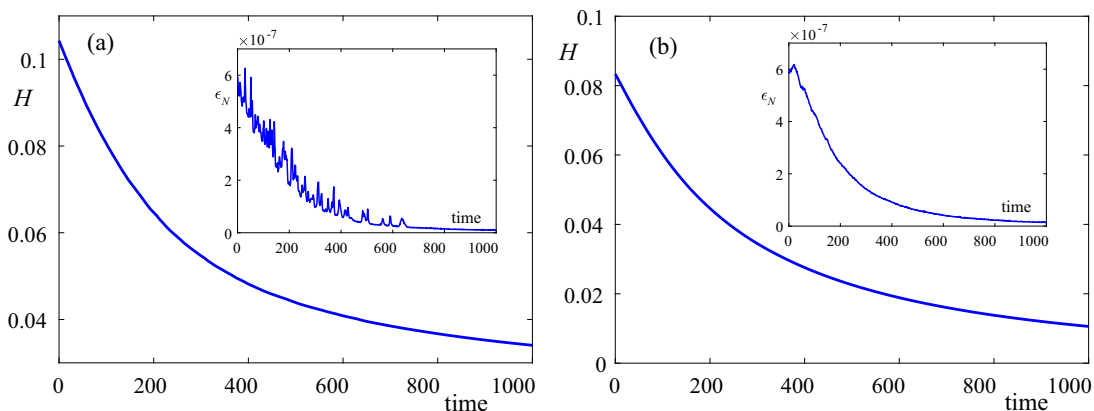


FIG. 4: (Color online) The evolution of the Hamiltonian is shown for $a = 2.5 \cdot 10^{-3}$ (a) and for $a = 0$ (b). Insets show the evolution of the instantaneous energy dissipation flux.

ESTIMATION OF THE KOLMOGOROV-ZAKHAROV CONSTANT

In this section we present two series of calculations of weakly dispersive and non-dispersive regimes of motion in order to calculate the KZ constants for both cases. Numerical experiments simulate decaying turbulence for $F_0 = 0$. The initial conditions were taken from the time instant, $t = 2000$, from Fig. 1 (a) and (b) corresponding to the quasi-stationary state. Calculations were carried out over a time interval, $T = 1000$. As can be seen from Fig. S 1, during this period of time the energy dissipates in several times, and the dissipation flux almost stops, i.e., the system becomes almost linear. The evolution of turbulence spectra in the decaying regime is shown in Fig. S 5. It can be seen that the spectrum evolution is self-similar with unchanged exponent $-9/2$, which corresponds to ZS spectrum. To directly calculate the KZ constants, we measure the energy spectrum constants, $E(k) = C_k k^{-3/2}$, in dependence on energy flux ϵ . The measured dependencies are in well agreement with $\epsilon^{1/2}$, see Fig. S 5 (c) and (d) for both weakly dispersive and non-dispersive regimes. The insets allow to directly estimate the values of KZ constants for two regimes: $C_{KZ} \approx 0.24$ (weakly dispersive) and $C_{KZ} \approx 0.1$ (non-dispersive).

ANALYSIS OF AN INDIVIDUAL JET

In this section, we present details of the analysis of an individual jet of the function $u(\mathbf{k})$ in Fourier space. To analyze the effect of divergence (wave diffraction), we consider a region in momentum space occupied by a separate jet. We consider a set of rays (an individual jet) passing through the origin of coordinates and extending along the

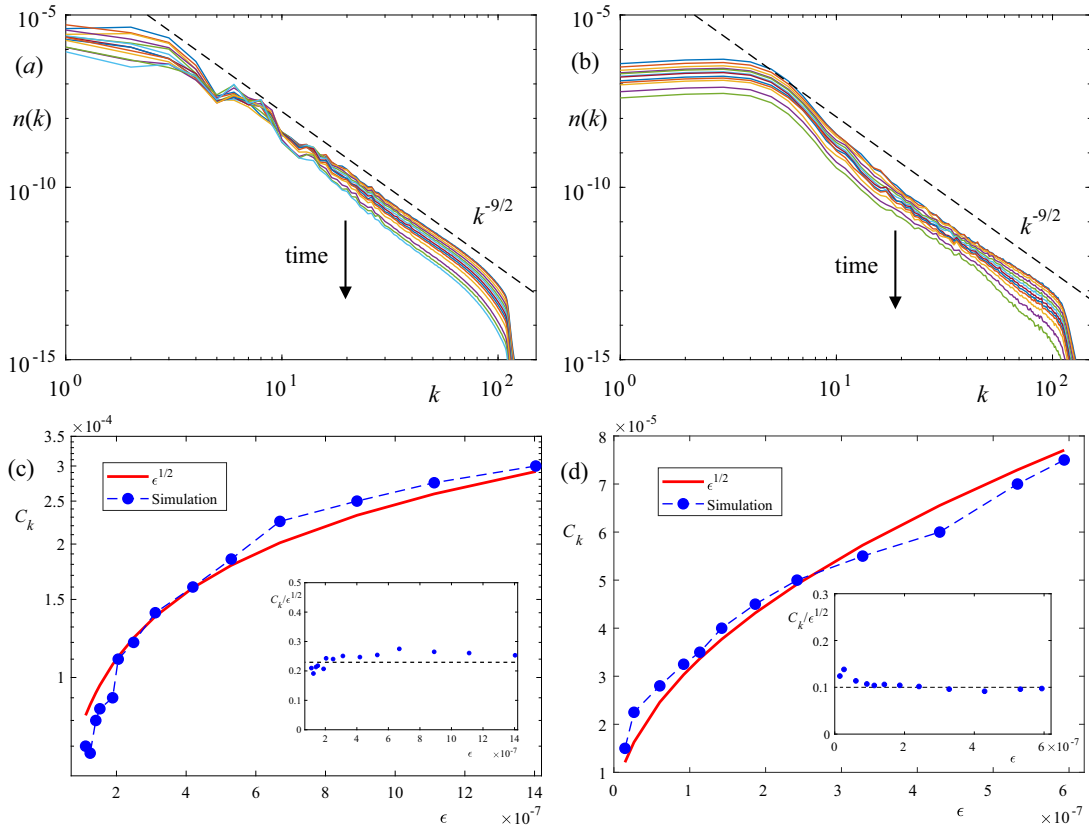


FIG. 5: (Color online) The spatial turbulence spectra in terms of wave action $n(k)$ are shown in dependence on time for $a = 2.5 \cdot 10^{-3}$ (a) and for $a = 0$ (b), black dashed line corresponds to KZ spectrum, $k^{-9/2}$. The coefficients C_k are shown as a function of the measured energy dissipation flux are shown for $a = 2.5 \cdot 10^{-3}$ (c) and for $a = 0$ (d). The red solid lines show the square root function $\epsilon^{1/2}$. Insets show compensated values of $C_k/\epsilon^{1/2}$ (KZ constant)

x -axis, see Fig. 2 (g) and (f) of the paper. As can be seen from the Fig. 2 (f), the rays diverge by an angle in the order of $\pi/10$. Fig. S 6 (a) shows the result of the filtration of initial spectrum by a cone with angle $\pi/10$. One can actually see that all the rays fit inside the cone area. Fig. S 6 (b) demonstrates the inverse Fourier transform of the filtered spectrum. It can be seen that the waves are not purely plane. The observed waves are weakly modulated in the direction perpendicular to the wave propagation. Applying the same filter to the function ϕ , we calculate the linear and nonlinear contributions of an individual jet to the Hamiltonian (8). Direct calculations show that the contribution of linear diffraction (wave divergence) turns out to be much greater than the energy of nonlinear wave interaction.

”BOTTLENECK” EFFECT

In this section we provide details of the analysis of the bottleneck effect. With this effect, energy accumulates in a region close to the dissipation scale k_d . The effect is observed with increasing amplitude of energy pumping. Fig. S 7 shows the Fourier spectra of the function $u(\mathbf{r})$ in the quasi-stationary regime for $F_0 = 2.5 \cdot 10^{-3}$ and $F_0 = 5 \cdot 10^{-3}$. It can be seen that as the energy pumping level increases, the beams in Fourier space become broader. With a further increase in the level of nonlinearity, rays from neighboring cones begin to intersect. At the same time, a peak near k_d appears in the turbulence spectra, see Fig. S 7 (c) and (d). To minimize the bottleneck effect, we introduce dissipation over the entire wavenumber range, i.e., $k_d = 1$. Thus, at a large pumping amplitude, the distribution of waves in Fourier space become quasi-isotropic, and the turbulence spectrum acquires shock-wave character, i.e., $E(k) \propto k^{-2}$.

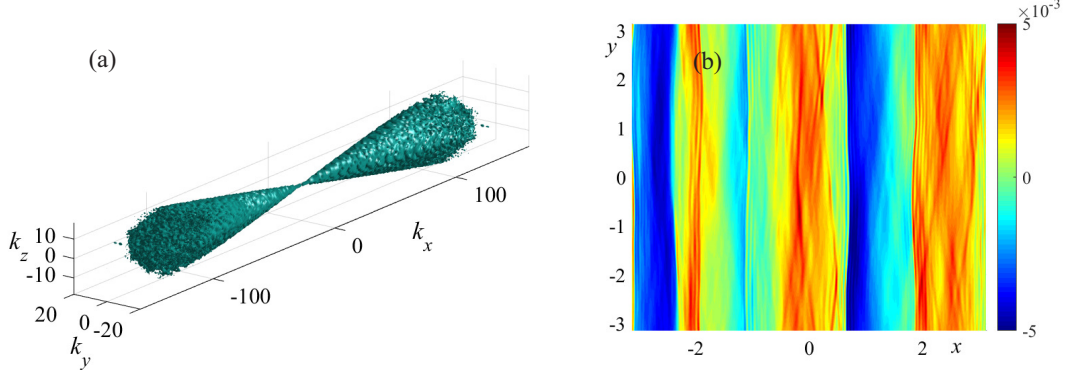


FIG. 6: (Color online) Isosurface of the Fourier spectrum $|u(\mathbf{k})| = 10^{-7}$ for the separate jet inside the angle $\pi/10$. The inverse Fourier transform of the jet is shown in $\{x, y\}$ plane at the moment $t = 2000$ corresponding to the quasi-stationary state.

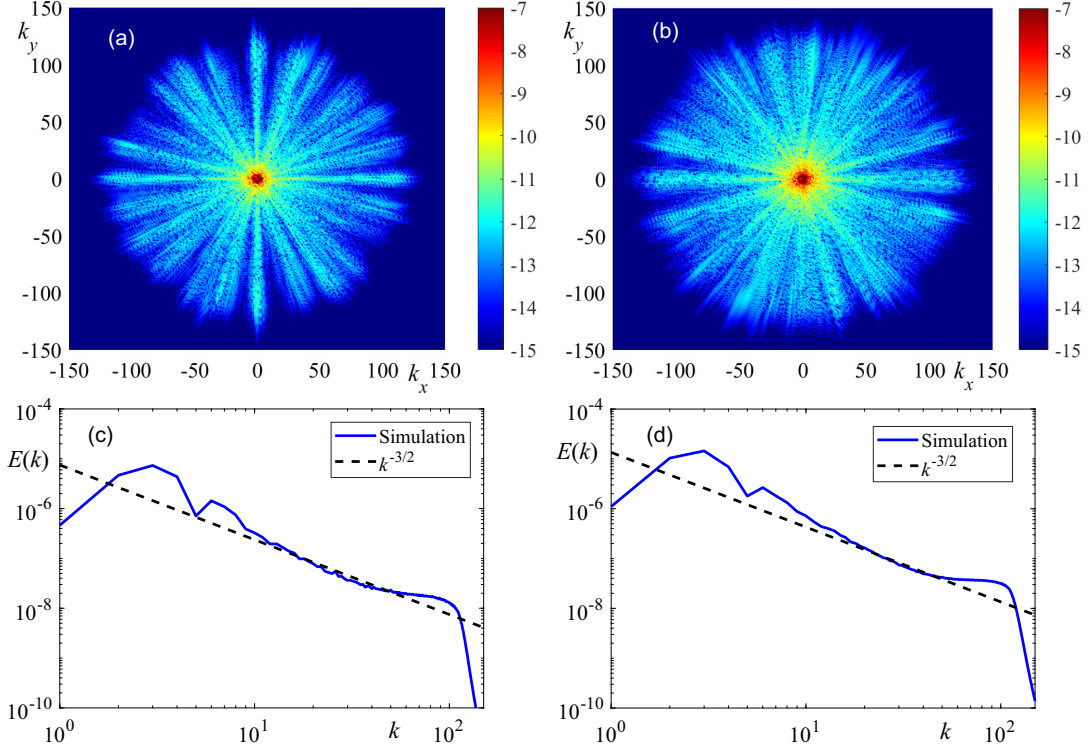


FIG. 7: (Color online) (a) and (b) Fourier spectra of $u(\mathbf{r})$ in $\{k_x, k_y\}$ plane. (c) and (d) The spatial turbulence spectrum in terms of spectral energy density. (a), (c) and (b), (d) correspond to $F_0 = 2.5 \cdot 10^{-3}$ and $F_0 = 5 \cdot 10^{-3}$, respectively.

CHARACTERISTIC NONLINEAR TIME COMPARISON

Fig. 3 (d) shows the space-time Fourier transform of the function $u(\mathbf{r}, t)$. One can indeed see that frequency broadening δ_ω is much higher in comparison with the weakly turbulent regime of motion shown in Fig 2 (d) and (h). The given space-time Fourier spectra allow to estimate the frequency broadening δ_ω (nonlinearity level) for each k [8]:

$$\delta_\omega = \left[\int_0^\infty (\omega - \omega_k)^2 |u(k, \omega)|^2 d\omega / \int_0^\infty |u(k, \omega)|^2 d\omega \right]^{1/2},$$

with $\omega_k = |\mathbf{k}|$. In fact, the quantity δ_ω determines the characteristic nonlinear time $\tau_{NL} = 1/\delta_\omega$. The applicability criterion for weak turbulence theory [1] can be written by the following way: $\tau_L/\tau_{NL} \ll 1$, where τ_L is the characteristic linear time, in our case $\tau_L = [\Omega_0^2 k/2]^{-1}$. Fig. S 8 shows the calculated time relation for weakly (WT) and strongly (ST) turbulent regimes. One can see that the difference between the parameters is near an order of magnitude. The value of τ_L/τ_{NL} for ST regime is above the threshold of weak turbulence applicability, whereas the measured time relation for WT regime is at least in five times less than unity, i.e., the criterion is satisfied in the weakly nonlinear case.

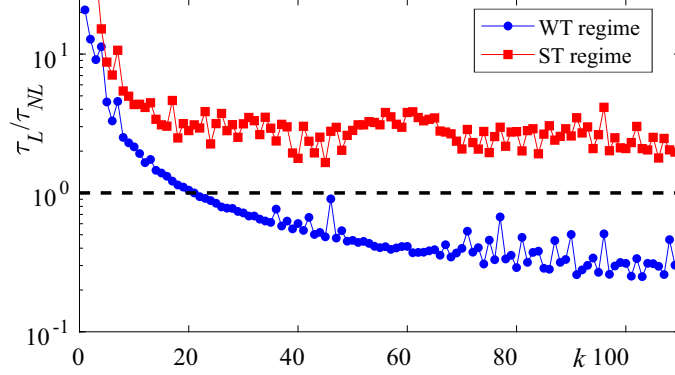


FIG. 8: Linear to nonlinear time ratios for $a = 0$.

* Electronic address: kochurin@iep.uran.ru

- [1] V.E. Zakharov, V.S. L'vov, G. Falkovich, Kolmogorov Spectra of Turbulence I: Wave Turbulence / Berlin Springer-Verlag, 1992.
- [2] S. Nazarenko, Wave Turbulence (Springer Berlin Heidelberg, series: Lecture Notes in Physics, 2011).
- [3] E. Falcon, N. Mordant, Annu. Rev. Fluid Mech. **54**, 1 (2022).
- [4] V.E. Zakharov, R.Z. Sagdeev, Sov. Phys. Dokl. **15**, 439 (1970).
- [5] A. C. Newell and P. J. Aucoin, J. Fluid Mech. **49**, 593 (1971).
- [6] V. S. L'vov, Y. L'vov, A. C. Newell, and V. Zakharov, Phys. Rev. E **56**, 390 (1997).
- [7] V. E. Zakharov, J. App. Mech. Tech. Phys., **6**(4), 22 (1965).
- [8] A. Griffin, G. Krstulovic, V. S. Lvov, S. Nazarenko, Phys. Rev. Lett. **128**, 224501 (2022).
- [9] V. E. Zakharov, E.A. Kuznetsov, Phys. Uspekhi **55**, 535-556 (2012).
- [10] B.B. Kadomtsev, V.I. Petviashvili, Dokl. Akad. Nauk SSSR **208**, 794 (1973).
- [11] E. A. Kuznetsov, JETP Lett. **80**, 83 (2004).
- [12] J. M. Burgers, Adv. Appl. Mech. **1**, 171 (1948).
- [13] E.A. Kochurin, E.A. Kuznetsov, JETP Lett. **116**, 863 (2022).
- [14] See Supplemental Material at <https://>
- [15] L.D. Landau and E. M. Lifshitz, Fluid Mechanics, p. 135 (Oxford: Pergamon Press, 1987).
- [16] C. Connaughton, P.L. Krapivsky, Phys. Rev. E **81**, 035303(R) (2010).
- [17] W. Walton, T. Minh-Binh, SIAM J. Sci. Comput. **45** (3), B467 (2023)